

# Towards Better Object Detection in Scale Variation with Adaptive Feature Selection

Zehui Gong<sup>a</sup>, Dong Li<sup>a,\*</sup>

<sup>a</sup>*Guangdong University of Technology*

---

## Abstract

It is a common practice to exploit pyramidal feature representation to tackle the problem of scale variation in object instances. However, most of them still predict the objects in a certain range of scales based solely or mainly on a single-level representation, yielding inferior detection performance. To this end, we propose a novel adaptive feature selection module (AFSM), to automatically learn the way to fuse multi-level representations in the channel dimension, in a data-driven manner. It significantly improves the performance of the detectors that have a feature pyramid structure, while introducing nearly free inference overhead. Moreover, we propose a class-aware sampling mechanism to tackle the class imbalance problem, which automatically assigns the sampling weight to each of the images during training, according to the number of objects in each class. Experimental results demonstrate the effectiveness of the proposed method, with 83.04% mAP at 15.96 FPS on the VOC dataset, and 39.48% AP on the VisDrone-DET validation subset, respectively, outperforming other state-of-the-art detectors considerably. The code is available at <https://github.com/ZeHuiGong/AFSM.git>.

*Keywords:* object detection, scale variation, multi-scale fusion

---

## 1. Introduction

In recent years, the performance of object detection consecutively improves, thanks to the carefully designed deep convolutional neural networks (CNNs) [1, 2, 3, 4] and high-quality large-scale benchmarks [5, 6]. However, these advanced detectors [7, 8, 9] are still struggling to tackle the wide range of variation in object scale, in real-world applications (see Fig. 1). To solve this problem, recent researches focus mainly on two possible strategies: image pyramid [10] and feature pyramid [11, 12, 13].

As for the image pyramid, a set of resized versions for one input image are sequentially sent to the detector at the testing phase. Therefore, the object scale will fall into an appropriate range at a specific image pyramid. However, this will increase the computational

---

\*Dong Li is the corresponding author.

*Email addresses:* [zehuigong@foxmail.com](mailto:zehuigong@foxmail.com) (Zehui Gong), [dong.li@gdut.edu.cn](mailto:dong.li@gdut.edu.cn) (Dong Li)



(a) large objects



(b) small objects

Figure 1: The size of objects varies significantly, posing a great challenge for object detection algorithms. In (a), the large object almost occupies 80% of an image, while in (b), the small ones can hardly be clearly captured without zooming.

cost considerably, making it unsuitable for real-world applications, especially for mobile devices. Conversely, another line of research constructs the feature pyramid based on the inherent multi-scale feature maps on the backbone network, which is memory efficient and consumes less computation. SSD [11] directly uses the multi-scale feature maps generated by the bottom-up pathway. FPN [12] constructs the feature pyramid by sequentially fusing high-level semantic information into low-level feature maps, with an additional top-down pathway and lateral connection.

Although FPN and other similar works [14, 15, 16, 17] achieve satisfactory performance, they still suffer from the following limitation. Specifically, each object in a specific range of scale is predicted based solely or mainly on the feature from a single level, while discarding the information in other levels, resulting in losing the chance to capture richer information. Generally, High-level features contain richer context and semantic information, with large receptive fields. This may be useful for small object prediction because the context information can be an additional cue for inferring the class of the small objects. Similarly, low-level features are spatially finer and, contain more details for high localization accuracy. Allowing large objects to access them is undoubtedly beneficial. It is hence achieving inferior detection performance to predict object instance in a certain range of size, based solely on single-level features. Some models attempt to solve this problem by enabling multi-level feature fusion. ASFF [18] fuses multi-level features via spatially point-wise addition. SFAM [19] re-weights the concatenated features at each scale with a SE module [20].

Another challenge for robust object detection is the problem of class imbalance, *i.e.*, the number of objects varies significantly from class to class, resulting in two sets of classes, the major and minor classes. This posts great challenges for the detection algorithms, since the training process can be dominated by the major classes, leading to rarely supervisory signals for the minor ones and consequently, harming the overall performance. Therefore, it is crucial to devise an effective mechanism to tackle the class imbalance problem.

In this paper, we propose a novel and effective adaptive feature selection module (AFSM), to tackle the problem of significant variation in object scale. The proposed method learns to

adaptively select useful information from multi-level representations in the channel dimension. Specifically, for the feature maps at a certain level, we first resize the feature maps from other levels into the same resolution. Then, the multi-level features are integrated by the corresponding selection weight (a learnable vector). Therefore, at each channel dimension, features at each level have a corresponding importance weight, thus automatically enhancing the discriminative clues beneficial to the following detection. The proposed approach is agnostic to the detector, *i.e.*, irrespective of one-stage or two-stage, and it can be applied to the detectors that have multi-level representations. Moreover, we propose a class-aware sampling mechanism (CASM) to solve the problem of class imbalance, which automatically assigns the sampling weight to each of the training images, according to the number of objects in each class. CASM increase the occurrence frequency of the minor class objects, resulting in more supervisory signals for these objects, hence improving the performance of minor classes considerably, as shown in Section 4.5.

The main contributions of this paper are summarized as follows:

1. We propose an adaptive feature selection module to adaptively select useful information across multi-scale representations, which enhances the ability of the model to cope with the variation in object scales.
2. Noticing that the problem of class imbalance restricts the performance of the detector, we propose a class-aware sampling mechanism to tackle the class imbalance problem, which can automatically assign the sampling weight to each of the images during training, according to the number of objects in each class.
3. Comprehensive experiments conducted on the VisDrone and PASCAL-VOC datasets confirm the effectiveness of our proposed method, which achieves state-of-the-art accuracy compared to other detectors, while still running in real-time.

In Section 2, we review the related works of object detection and feature pyramid structure. The details of the proposed algorithm are illustrated in Section 3. And we describe the implementation details and the experimental results in Section 4. Finally, a brief conclusion of our work is given in Section 5.

## 2. Related Work

**Object detection** Formally, the modern object detection methods can be categorized into two types: one-stage pipeline [8, 11, 9] and two-stage pipeline [21, 7, 22]. One-stage detectors achieve real-time performance by outputting the detection results directly without proposal generation procedure. Specifically, YOLO [8] regresses bounding boxes and class probabilities in a single efficient backbone network. SSD [11] covers objects of various sizes by adjusting the output bounding boxes on the default boxes over multiple feature maps. RetinaNet [9] settles the extreme foreground-background class imbalance, thus achieving better performance than two-stage object detectors. Alternatively, two-stage detectors obtain higher accuracy by combining the region proposal stage and classification stage. Specifically, Faster R-CNN [7] introduces a region proposal network (RPN), which simultaneously

predicts bounding boxes and objectness scores to achieved further speeds-up. Double-Head RCNN [22] handles the classification in a fully connected head while regressing the bounding in a convolution head. Recently, some researches [23, 24, 25, 26] provide a different view of objects, by detecting keypoints of the bounding box.

**Feature pyramid** Feature pyramid representations, *i.e.*, multi-level feature maps, is a basic solution to tackle the variation in object scale. Skip connection [27] and hyper-column [28] are the early attempts to integrate multi-level feature to generate more representative feature maps. After that, multi-scale prediction [11, 12, 29, 30] begins to emerge, because of the lightweight property, higher accuracy, and faster inference compared to image pyramids. SSD [11] predicts class scores and bounding boxes respectively at multiple feature levels. FPN [12] introduces a top-down pathway, and a lateral connection to sequentially merge high-level semantic information into the low-level features, building multi-level representations for the following detection head. PANet [29] adds an extra bottom-up pathway on the basis of FPN to shorten the distance between high-level and low-level features. In BiFPN [30], multiple PANet-like structures with scale-wise level re-weighting is proposed, to fuse feature maps from different scales. Another line of works [31, 32] employs the Neural Architecture Search (NAS) algorithm to automatically find the powerful architecture for multi-level representations, improving the performance considerably.

**Selection of multi-scale features** Besides the generation of multi-level features, some of the researches [18, 19, 33] make a step forward and, delve into the mechanism of how to select useful information across various feature levels. In [33], a learnable gating unit is proposed to control the flow of information in single-level skip connection, in the U-Net architecture for visual counting. Zhao et al. [19] propose a scale-wise feature aggregation module (SFAM) to execute channel-wise attention on the concatenated multi-scale feature maps, where the attention weights are generated by the squeeze and excitation (SE) module [20]. In [18], the point-wise attention weights are used for multi-level feature fusion, where a  $1 \times 1$  conv is employed to generate the weight at each level, following by a softmax layer for normalizing.

The spatially point-wise addition proposed in [18] is not effective enough for multi-level feature selection and, introduces more computational cost (*i.e.*, several  $1 \times 1$  convs for generating fusion weights). In this paper, by regarding the selection weight at each level as a learnable vector for channel-wise multi-level feature fusion, AFSM can automatically learn the distribution of object size over the whole dataset (as showed in Section 4.5), which makes the selection process more stable and effective. It seems that SFAM [19] shares the same spirit of our work. However, we emphasize that SFAM only executes channel-wise attention at a single level, on the concatenated feature maps, instead of adaptively selecting useful information across various levels.

### 3. The Proposed Method

The overall framework of our approach is shown in Fig. 2. In this section, we first introduce the baseline network architecture of our proposed method, which is based on the effective anchor-free detector, *i.e.*, CenterNet [25]. Then, we move on to push the original

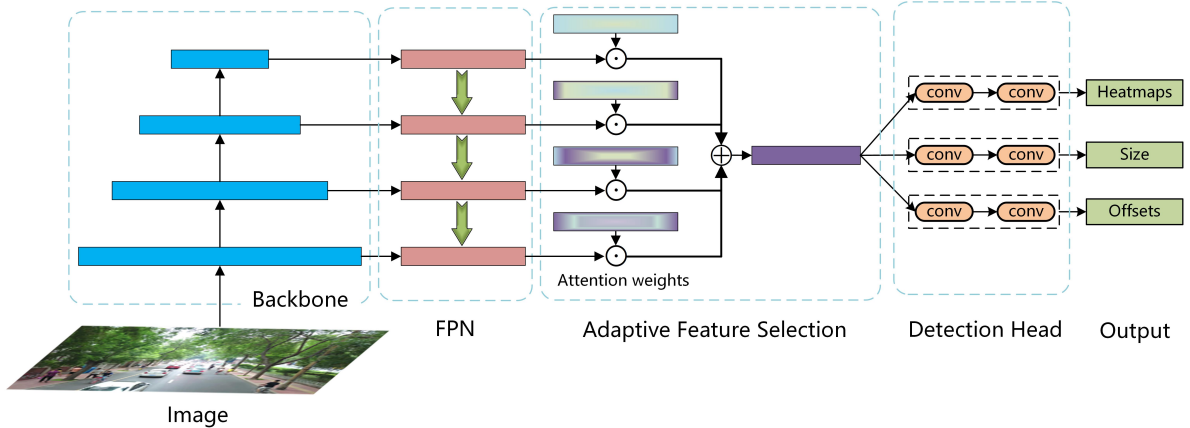


Figure 2: The overall framework of our proposed method. The backbone network is followed by the feature pyramid network (FPN) [12] for multi-scale feature generation. Then, the adaptive feature selection module is employed to adaptively select the most useful information for the subsequent detection task. Finally, the model outputs the center locations and the corresponding offsets, as well as the object sizes, to form the final bounding boxes.  $\odot$  is the broadcast element-wise multiplication, and  $\oplus$  means the element-wise addition. For simplicity, we show the procedure of multi-scale feature fusion in a certain level only.

baseline to a stronger version, by employing the recently advanced tricks, such as mixup [34] and global context block (GCB) [35], and by proposing two effective techniques, class aware sampling mechanism and modified GIOU [36] loss. Finally, we describe our proposed adaptive feature selection module in detail, which adaptively selects features from multi-scale representations in the channel dimension.

### 3.1. Network Architecture

We adopt CenterNet [25] as our baseline method, because of its simplicity and high efficiency. CenterNet presents a new representation for detecting objects, in terms of the center location of a bounding box. Other object properties, *e.g.*, object size, and center offset, are regressed directly using the image features from the center locations. Let  $(ct_x, ct_y, w, h, \epsilon_x, \epsilon_y)$  be one output that generates from the model. Then, we construct the bounding box  $\mathcal{B} \in R^4$  by:

$$\mathcal{B} = \begin{cases} x_1 = ct_x + \epsilon_x - w/2, \\ y_1 = ct_y + \epsilon_y - h/2, \\ x_2 = ct_x + \epsilon_x + w/2, \\ y_2 = ct_y + \epsilon_y + h/2. \end{cases} \quad (1)$$

where  $(ct_x, ct_y)$  is the center location of an object and,  $(\epsilon_x, \epsilon_y)$  is the offset prediction used to slightly adjust the center point.  $(w, h)$  is the object size prediction and,  $(x_1, y_1)$  and  $(x_2, y_2)$  are the top-left and bottom-right corners of the bounding box. The overall training objective of CenterNet is given as follows:

$$L = L_{ct} + \lambda_{size}L_{size} + \lambda_{off}L_{off} \quad (2)$$

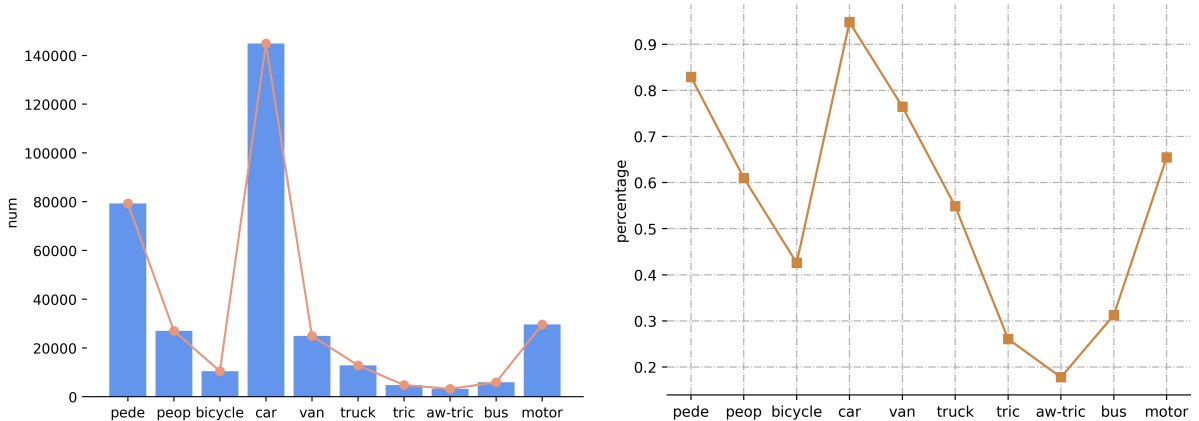


Figure 3: The analysis of category statistics on the VisDrone-DET training set. **Left:** The total number of object instances for each category varies significantly from class to class. **Right:** The ratio of images contains the corresponding class. The ratio of images containing ‘awning-tricycle’ is less than 20%

where  $L_{ct}$  is the loss for center location estimation, which is a variant of the focal loss [9].  $L_{off}$  is the L1 loss for center offset regression.  $L_{size}$  is a modified version of the GIOU loss that fits in the object size regression of CenterNet, and we will describe it in detail in section 3.2.  $\lambda_{size}$  and  $\lambda_{off}$  are hyper-parameters, which are all set to 1.0 in our experiments, unless otherwise specified.

### 3.2. Stronger Baseline

CenterNet mainly contains two components: a backbone network (usually the Hourglass-104 [37]) and a detection head with three parallel branches to predict the center location, offset, and object size (*i.e.*,  $w$  and  $h$ ) of a bounding box. In this paper, we employ ResNet [1] as the backbone network and, use feature pyramid network (FPN) to generate multi-scale feature maps. Moreover, we employ the recently advanced training tricks [34, 35], and propose two effective approaches, to further improve the performance of the baseline method.

**Advanced techniques** In [38], mixup algorithm [34] is demonstrated to be an effective data augmentation method, to improve the robustness of the model by a stochastic linear interpolation between two training examples. Let  $I$  be one input image, and  $B = \{x_1^i, y_1^i, x_2^i, y_2^i, c^i\}_{i=1}^n$  denote the corresponding bounding box annotation of that image, and  $n$  is the number of the boxes. Then, the mixup operation can be formulated as follows:

$$\lambda_1 \sim \text{Beta}(\eta, \eta), \quad (3)$$

$$\lambda_2 = \min(\max(0, \lambda_1), 1), \quad (4)$$

$$I = \lambda_2 I_1 + (1 - \lambda_2) I_2, \quad (5)$$

$$B = \text{concat}(B_1, B_2). \quad (6)$$

---

**Algorithm 1** Detailed procedures of class-aware sampling mechanism

---

**Input:**

The list of class labels for each of the training images,  $G = \{G_i\}_{i=1}^N$ , where  $G_i = \{c_j\}_{j=1}^n$ ,  $N$  is the number of training images,  $n$  the number of objects in each image.

The number of training classes,  $K$

**Output:**

The list of sampling ratios for each image,  $S = \{s_1, \dots, s_N\}$ , used for training sampling.

```
1:  $S \leftarrow \emptyset, M \leftarrow \emptyset$ 
2: for each  $k \in [1, K]$  do
3:    $M(k) \leftarrow 0$  // Initialize the number of objects in each class to 0.
4: end for
5: for  $G_i \in G$  do
6:   // Counting the number of object instance  $t$  in class  $k$ , in image  $i$ 
7:   for  $k, t \in \text{counter}(G_i)$  do
8:      $M(k) \leftarrow M(k) + t$ 
9:   end for
10: end for
11: for each  $i \in [1, N]$  do
12:    $s \leftarrow 0$ 
13:   // Enumerate the set of unique classes in image  $i$ 
14:   for  $k \in \text{unique}(G_i)$  do
15:      $s \leftarrow s + \frac{1}{M(k)}$ 
16:   end for
17:    $S \leftarrow S \cup \{s\}$ 
18: end for
19: // Normalize the sampling ratios
20:  $S \leftarrow S / \text{sum}(S)$ 
21: return  $S$ 
```

---

Where  $\text{concat}(\cdot)$  means the concatenation operation of the bounding box annotation between two mixup images.

Besides, the long-range pixels in the image may be still correlated. For example, an object is less likely to be a car when the background is the sea. Therefore, it is important to model the long-range relations between pixels. We adopt the global context block (GCB) [35], which is an effective module to model the global context and, is much lightweight compared to NLNet [39].

**Class-aware training sampling** In real-world applications, imbalanced data is ubiquitous, where the number of an object instance in each class varies significantly (see Fig. 3). This posts a great challenge for the detector, since the training process can be dominated by the major classes, leading to rarely supervisory signals for the minor ones. To address this issue, we propose a novel re-weighting mechanism, *i.e.*, class-aware sampling mechanism (CASM), to automatically assigns the sampling ratio for each image in the training set, instead of the uniform sampling. Alg. 1 shows the detailed procedures of CASM, where the sampling ratio for each of the images is computed automatically, according to the occurrence frequency of each class in the dataset.

**Modified GIOU** CenterNet uses L1 loss for object size regression, which is sensitive to the

---

**Algorithm 2** Workflow of the modified GIOU loss

---

**Input:**  $O^p = \{r_i^p, \dots, r_N^p\}$ ,  $O^g = \{r_i^g, \dots, r_N^g\}$ , and  $F \in \{0, 1\}^N$   
 $O^p = \{r_i^p, \dots, r_N^p\}$  is the set of predicted object size  
 $O^g = \{r_i^g, \dots, r_N^g\}$  is the set of ground-truth object size  
 $r_i^p = (w_i^p, h_i^p)$ ,  $r_i^g = (w_i^g, h_i^g)$   
 $N$  is the maximum number of training objects in one image, *e.g.*,  $N = 128$   
 $F$  is a mask that each element indicates the object is foreground or background.

**Output:**  $L_{size}$

- 1: initialize  $L_{size} \leftarrow 0$ .
- 2: **for** each  $i \in [1, N]$  **do**
- 3:    $w_i^p \leftarrow \exp(w_i^p)$ ,  $h_i^p \leftarrow \exp(h_i^p)$ .
- 4:   Getting intersection box size:  $t_w \leftarrow \min(w_i^p, w_i^g)$ ,  $t_h \leftarrow \min(h_i^p, h_i^g)$ .
- 5:   Getting the smallest enclosing box size:  $c_w \leftarrow \max(w_i^p, w_i^g)$ ,  $c_h \leftarrow \max(h_i^p, h_i^g)$ .
- 6:   Calculating area of  $r_i^p$ :  $A^p \leftarrow w_i^p \times h_i^p$ .
- 7:   Calculating area of  $r_i^g$ :  $A^g \leftarrow w_i^g \times h_i^g$ .
- 8:   Calculating area of smallest enclosing box:  $A^c \leftarrow c_w \times c_h$ .
- 9:   Calculating area of intersection box:  $A^t \leftarrow t_w \times t_h$ .
- 10:    $IoU \leftarrow \frac{A^t}{\mathcal{U}}$ , where  $\mathcal{U} = (A^p + A^g - A^t)$ .
- 11:    $GIoU \leftarrow IoU - \frac{A^c - \mathcal{U}}{A^c}$ .
- 12:   // Multiply by the mask  $F(i)$ , where the loss for background object is 0.
- 13:    $L_{size} \leftarrow L_{size} + (1 - GIoU) \times F(i)$
- 14: **end for**
- 15: **return**  $L_{size}$ .

---

variation in object size and, separately regresses the width and height of an object, hence overlooking the correlation between properties of the same object. Conversely, GIOU loss [36] considers the optimization as a whole, and is irrelevant to the object size. However, GIOU loss is first proposed for the anchor-based methods, which can not be applied to the CenterNet directly. Therefore, we make some modifications to the GIOU loss. The entire workflow of computing the modified GIOU (M-GIOU) loss is illustrated in Alg. 2, where an additional mask  $F \in \{0, 1\}^N$  is introduced to filter out the background object during back-propagation.

### 3.3. Adaptive Feature Selection Module

The object scales vary significantly in real-world scenarios, posing great challenges for detection algorithms. It is hence vital to develop an approach, to cope with a wide range of variation in object scales. Therefore, we propose an adaptive feature selection module (AFSM) to adaptively learn the importance weights, for fusing feature maps from different feature levels. As shown in Fig. 2, the pipeline is consists of two steps: feature resizing and adaptive feature selection.

**Feature resizing.** Formally, a list of multi-scale features is given as  $X = \{X^1, \dots, X^l, \dots\}$ , where  $X^l$  is the feature maps at level  $l$ , whose resolution is  $1/2^l$  of the input image. For

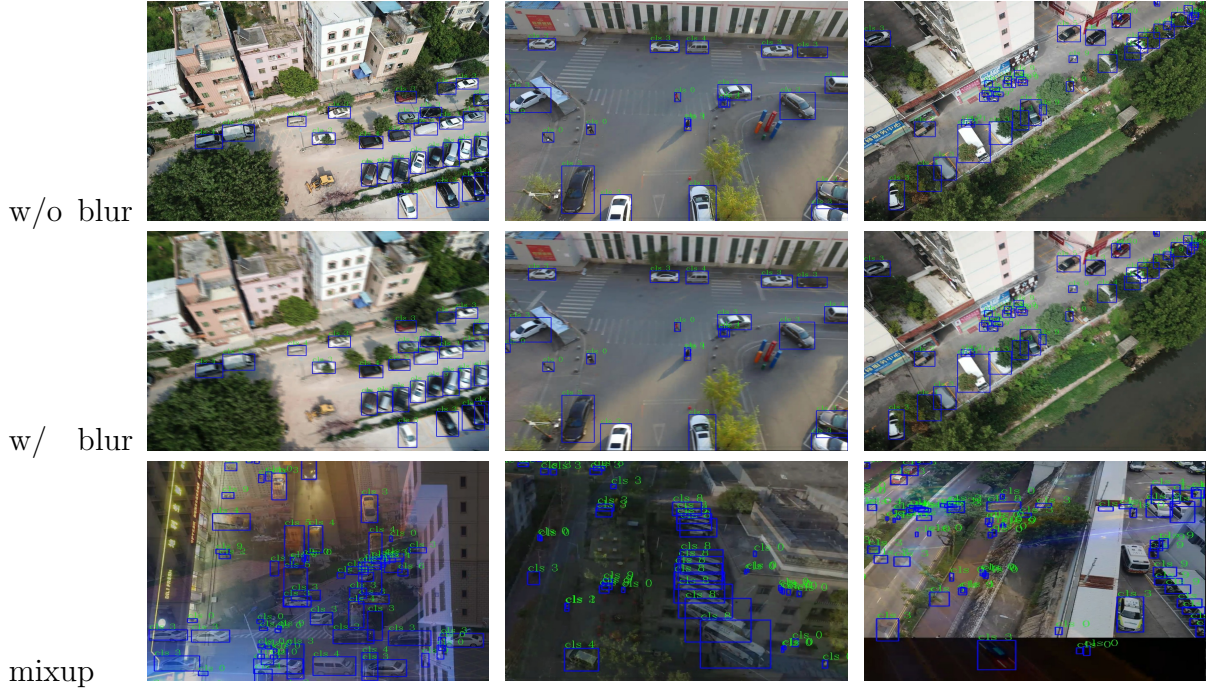


Figure 4: Visualization of the images that use random blurring and mixup data augmentation. By applying these techniques, the distribution of the training samples is significantly expanded, thus leading to stronger generalization ability of the model.

feature maps at level  $l$ , we first resize it with a scale factor of  $2^{|l-k|}$ , to the same resolution of the feature maps at level  $k$ , where  $k$  is the target level, *e.g.*,  $k = 3$ . As the output stride is of 4 in CenterNet, we resize the feature maps after feature selection, to ensure the resolution is of 1/4 of the input image. Specifically, the nearest interpolation operation is adopted to resize the features respectively at each scale.

**Adaptive feature selection.** Let  $\hat{X} = \{\hat{X}^1, \dots, \hat{X}^l, \dots\}$  be the feature maps after resizing. We propose to fuse features across various resolutions as follows:

$$Y_i = \sum_l \hat{X}_i^l \cdot \alpha_i^l, \quad (7)$$

where  $Y_i$  implies the  $i$ -th channel of the output feature maps among spatial positions.  $\alpha_i^l$  refers to the channel importance weight that controls the contribution of feature maps at level  $l$  to the prediction of the bounding box. Note that  $\alpha_i^l$  is a simple scalar variable, sharing across all the spatial positions. Softmax  $\alpha$  operation is employed to ensure  $\sum_l \alpha_i^l = 1$ , as follows:

$$\alpha_i^l = \frac{\exp(\beta_i^l)}{\sum_k \exp(\beta_i^k)} \quad (8)$$

where  $\beta_i^l$  is a learnable scalar variable, which is initialized to one and, can be adaptively learned by the network through standard back-propagation.

Table 1: The Comparison with state-of-the-arts on the VisDrone-DET *validation* subset. All models are trained on VisDrone-DET train set. † implies that the multi-scale inference is employed.

Method	Backbone	AP	AP <sup>50</sup>	AP <sup>75</sup>	AR <sup>1</sup>	AR <sup>10</sup>	AR <sup>100</sup>	AR <sup>500</sup>
Cascade R-CNN [21]	ResNet50	24.10	42.90	23.60	0.40	2.30	21.00	35.20
Faster R-CNN [7]	ResNet50	23.50	43.70	22.20	0.34	2.20	18.30	35.70
RetinaNet [9]	ResNet50	15.10	27.70	14.30	0.17	1.30	24.60	25.80
FCOS [41]	ResNet50	16.60	28.80	16.70	0.38	2.20	24.40	24.40
HFEA [42]	ResNeXt101	27.10	-	-				
HFEA [42]	ResNeXt152	30.30	-	-				
ClusDet [43]	ResNeXt101	32.40	56.20	31.60				
CPEN+FPEN [44]	Hourglass104	36.70	53.20	<b>39.50</b>				
DMNet+DSHNet [45]	ResNet50	30.30	51.80	30.90				
DSOD [46]	ResNet50	28.80	47.10	29.30				
HRDNet [47]	ResNet18+101	28.33	49.25	28.16	0.47	3.34	36.91	36.91
HRDNet† [47]	ResNeXt50+101	35.51	62.00	35.13	0.39	3.38	30.91	46.62
Ours	CBResNet50	33.95	60.46	32.69	0.66	7.25	40.28	49.84
Ours†	CBResNet50	37.62	65.41	37.06	0.62	7.21	43.21	56.26
Ours	CBResNet50+DCN	35.43	61.88	34.60	0.80	7.77	41.77	51.48
Ours†	CBResNet50+DCN	<b>39.48</b>	<b>66.98</b>	39.45	<b>0.82</b>	<b>7.94</b>	<b>44.76</b>	<b>58.46</b>

With our proposed feature selection module, the features at different levels are aggregated adaptively. The output  $Y$  is then used for the subsequent object detection following the same pipeline of CenterNet.

## 4. Experiments

### 4.1. Datasets

We select two challenging datasets to validate the effectiveness of our proposed algorithm, VisDrone [40] and PASCAL-VOC [6].

**VisDrone** VisDrone is a very challenging dataset, with a wide range of variation in scale, lighting condition, scenario, viewpoint, and blurring. This dataset contains a total of 10209 images for object detection on drones, which are captured by various drone platforms, and from 14 different cities in China, including various scenarios. Ten object categories, *e.g.*, car and van, are considered for evaluation. Specifically, 10209 images are split into four subsets, including 6471 images in the *training* subset, 548 in the *validation* subset, 1610 in the *test-dev* subset, and 1580 in the *test-challenge* subset.

**PASCAL-VOC** VOC is a popular dataset for object detection. The union set of 2007 and 2012 train&val is used for training, including 16551 images. The evaluation is performed on the VOC 2007 test set, with 4962 testing images, and a total of 20 categories.

Table 2: Comparison results of various algorithms on the VisDrone-DET *test-challenge* subset. † implies that the multi-scale inference is employed.

Method	AP	AP <sup>50</sup>	AP <sup>75</sup>	AR <sup>1</sup>	AR <sup>10</sup>	AR <sup>100</sup>	AR <sup>500</sup>
DPNet-ensemble	29.62	54.00	28.70	0.58	3.69	17.10	42.37
RRNet	29.13	55.82	27.23	1.02	8.50	35.19	46.05
ACM-OD	29.13	54.07	27.38	0.32	1.48	9.46	44.53
S+D	28.59	50.97	28.29	0.50	3.38	15.95	42.72
BetterFPN	28.55	53.63	26.68	0.86	7.56	33.81	44.02
HRDet+	28.39	54.53	26.06	0.11	0.94	12.95	43.34
CN-DhVaSa	27.83	50.73	26.77	0.00	0.18	7.78	46.81
MSC-CenterNet	31.13	54.13	31.41	0.27	1.85	6.12	50.48
CenterNet+	30.94	52.82	31.13	0.27	1.84	5.67	50.93
PG-YOLO	26.05	49.63	24.15	<b>1.45</b>	9.20	33.65	42.63
Ours†	<b>32.34</b>	<b>56.46</b>	<b>32.39</b>	1.20	<b>9.45</b>	<b>38.55</b>	<b>51.61</b>

#### 4.2. Evaluation Metrics

For the VisDrone dataset, we use the same evaluation protocol proposed in [40], which is almost the same as COCO [5], except for reporting an additional  $AR^{\max=500}$  score. The mean average precision (mAP) over thresholds of  $IoU = 0.5 : 0.05 : 0.95$  is reported. Moreover, we report the  $AP^{IoU=0.5}$ ,  $AP^{IoU=0.75}$ ,  $AR^{\max=1}$ ,  $AR^{\max=10}$ , and  $AR^{\max=100}$  scores. For the VOC dataset, we use mAP at IOU threshold 0.5 as the evaluation metric.

#### 4.3. Implementation Details

**Training** We implement our model on the deep-learning framework of PaddlePaddle [48]. For the VisDrone dataset, the input resolution of the network is set to  $1023 \times 767$  during training, which results in an output resolution of  $256 \times 192$ . For the VOC dataset, the training resolution is fixed at  $512 \times 512$ . We use extensive data augmentation techniques to reduce the risk of overfitting. For standard data augmentation, we adopt random cropping, random scaling, random flipping, random blurring, and random color jittering. Moreover, we use the mixup algorithm [34] to improve the generability of the model. Some example images of our data augmentation techniques are showed in Fig. 4.

Adam [49] algorithm is adopted to optimize the overall training objective. We train our model on a V100 GPU with a batch size of 8. Note that for ablation study, we train our model for 50k iterations, with an input resolution of  $511 \times 511$ , to save computational resources. When comparing to other state-of-the-arts, we train the model for a total of 120k iterations. The learning rate starts from  $2e-4$  and, is decayed by cosine annealing strategy.

**Inference** Following the setting of CenterNet, we use three levels of test augmentation, *i.e.*, no augmentation, flipping, and multi-scale (1.0, 1.25, 1.5, and 1.8) test augmentation. Specifically, for flipping test augmentation, the network predictions of the flipped and non-flipped inputs are average before decoding. For multi-scale test augmentation, non-maximum suppression (NMS) is further applied to filter out the duplicate predictions.

Table 3: The performance comparison on VOC 2007 test set, in terms of mAP (%).

Method	Backbone	Input size	mAP	FPS
Faster R-CNN [7]	ResNet101	1000×600	76.4	5
R-FCN [50]	ResNet101	1000×600	80.5	9
OHEM [51]	VGG-16	1000×600	74.6	-
R-FCN [50]	ResNet101+DCN	1000×600	82.6	-
CoupleNet [52]	ResNet101	1000×600	82.7	8.2
DeNet(wide) [53]	ResNet101	512×512	77.1	33
FPN-Reconfig [54]	ResNet101	1000×600	82.4	-
Yolov2 [55]	DarkNet19	544×544	78.6	40
SSD [11]	VGG-16	513×513	78.9	19
DSSD [14]	VGG-16	513×513	81.5	5.5
RefineDet [16]	VGG-16	512×512	81.8	24
CenterNet [25]	ResNet101	512×512	78.7	30
CenterNet [25]	DLA	512×512	80.7	33
HRDNet [47]	ResNeXt50+101	2000×1200	82.4	-
Ours	CBResNet50	511×511	78.2	25.08
Ours	CBResNet50+DCN	511×511	81.05	21.98
Ours	ResNet101+DCN	511×511	<b>83.04</b>	15.96

#### 4.4. Comparison with state-of-the-arts

We first demonstrate the advancement of our proposed method on the very challenging VisDrone dataset. Then we move on to prove the strong generality of our model on the VOC dataset.

**VisDrone** The comparison results with other state-of-the-art methods on VisDrone2019 DET *test-challenge* and *validation* subset is showed in Table 2 and Table 1, respectively. Our model achieves the best performance among other detectors, with an AP score of 32.34% on the *test-challenge* subset, and 39.48% AP on the *validation* subset, respectively. This outperforms other algorithms by a large margin, with an improvement of 7.08% AP over ClusDet [43], demonstrating the effectiveness of our proposed model. It is worth noting that the average recall (AR) obtained by the proposed model also outperforms other methods at all levels (from AR<sup>1</sup> to AR<sup>500</sup>), which shows that our model can better cope with the variation in object scale (find out more object instance), with the help of adaptive feature selection module.

**PASCAL-VOC** Table 3 tabulates the results of various state-of-the-art methods on VOC dataset. Note that flipping test augmentation is used by default. Our method achieves the best performance, with an mAP score of 83.04%, while still running in real-time (15.96 FPS). DSSD yields 81.5% mAP, which is comparable to our method using CBResNet50 [56] as the backbone, whereas the inference speed is approximately one third of ours (5.5 FPS *vs.* 21.98 FPS). Therefore, our method performs well on the balance of speed and accuracy.

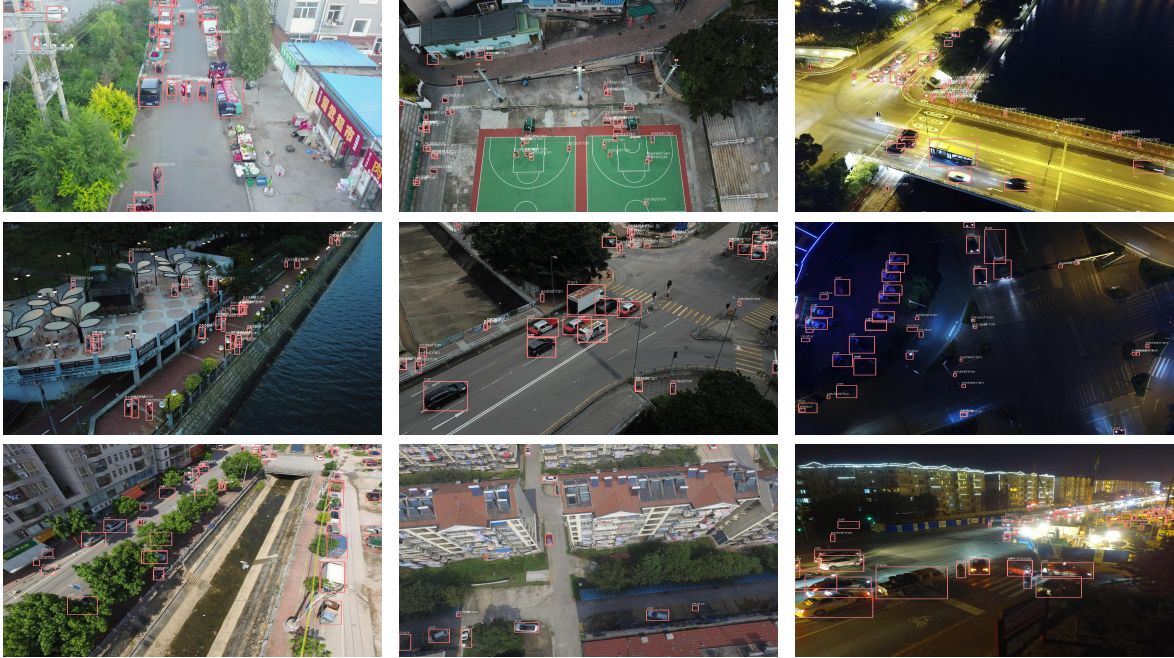


Figure 5: Qualitative visualization of the detection results on VisDrone-DET *test-challenge* subset. Our model is capable of dealing with objects with a wide range of variation in shape, viewpoint, lighting condition, and blurring, etc.

#### 4.5. Ablation Studies

**Strong baseline** The contribution of each advanced components to our baseline detector is tabulated in Table 4, where GCB denotes the global context block [35], CASM is the class-aware sampling mechanism, and M-GIOU denotes the modified GIOU loss for object size regression. As shown in Table 4, all the techniques boost the performance, *e.g.*, adding CASM to the baseline method improves the AP from 25.92% to 26.71%, with an increase of 0.79%. Thanks to these techniques, we produce a stronger baseline that delivers an AP score of 28.34%, an improvement of 2.42% over the CenterNet baseline. It is worth noting that the improvement is almost cost-free, as mixup, CASM, and M-GIOU do not introduce any extra computational cost, and GCB owns the light-weight property. Therefore, the final baseline still runs in an FPS of 20.76 on a single GPU of NVIDIA Tesla V100.

**Influence of the regression weight  $\lambda_{size}$**  Further on we study the influence of the regression weight on the detector accuracy, as shown in Table 5.  $\lambda_{size} = 1.0$  yields good results, with an AP score of 26.85%. For larger ( $\lambda_{size} = 5.0$ ) or smaller ( $\lambda_{size} = 0.2$ ) values, the AP degrades a little bit, with 0.23% and 0.57% AP, respectively. This shows that M-GIOU loss is not much sensitive to the variation of  $\lambda_{size}$ .

**Channel fusion vs. Spatial fusion** To analyze the effectiveness of the proposed AFSSM, we further report the results of ASFF [18] based on the CenterNet baseline. As shown in Table 6, applying ASFF to the baseline improves the performance by 3.23% AP, showing that fusing multi-level representations via point-wise spatial addition helps the model to tackle the variation in object scale. However, adding AFSSM to the baseline boosts the performance

Table 4: Effect of each advanced techniques on the baseline, in terms of APs (%). All models employ ResNet50 [1] as backbone network. FPS are reported on VisDrone2019 DET *validation* subset, keeping the original resolution for testing.

CenterNet	GCB	mixup	CASM	M-GIOU	AP	AP <sup>50</sup>	AP <sup>75</sup>	FPS
✓					25.92	46.81	24.75	23.20
✓	✓				27.51	49.11	26.66	20.76
✓		✓			26.94	47.87	26.14	22.58
✓			✓		26.71	47.76	25.71	22.58
✓				✓	26.85	48.04	26.00	22.58
✓	✓	✓	✓	✓	28.34	49.92	27.92	20.76

Table 5: The influence of  $\lambda_{size}$  on our model.

$\lambda_{size}$	AP	AP <sup>50</sup>	AP <sup>75</sup>	AR <sup>1</sup>	AR <sup>10</sup>	AR <sup>100</sup>	AR <sup>500</sup>
0.2	26.28	47.74	25.21	0.62	7.01	35.76	35.76
1.0	<b>26.85</b>	<b>48.04</b>	<b>26.00</b>	<b>0.72</b>	<b>7.03</b>	<b>36.23</b>	<b>36.23</b>
5.0	26.62	47.18	25.94	0.58	6.75	36.05	36.05

by 4.02% AP, with an increase of 0.79% AP compared to ASFF. This implies that fusing features across feature levels by re-weighting the importance distribution over the channel dimension may be more suitable and effective than the spatial dimension. Moreover, instead of using several  $1 \times 1$  convs to generate fusion weights for a specific image, we regard the fusion weight as a learnable vector. This enables AFSM to learn the distribution of object size over the whole dataset, which makes the selection process more stable and effective.

**How to obtain adaptive feature selection weights** For obtaining the weights  $\alpha^l \in \mathbb{R}^d$  to select representative features across multi-scale levels, we evaluate the performance based on three kinds of methods, where  $d$  is the number of channels in feature maps  $X^l$ . The difference between these methods is the ways to obtain  $\beta^l$  in Eq. 8. The first is a learnable vector, which is initialized to one and, can be updated by the standard back-propagation algorithm. For the second version, we first pool the feature maps  $X^l$  using global average pooling (GAP) operation, obtaining  $X_p^l \in \mathbb{R}^d$ . Then each of the pooled features is followed by a fully connected (FC) layer, to obtain  $\beta^l$ , which is given as follows:

$$X_p^l = \text{GAP}(X^l) \quad (9)$$

$$\beta^l = \text{FC}(X_p^l) \quad (10)$$

The third version uses GAP to pool the feature maps  $X^l$ . Then we concatenate the features from all levels, denoted as  $X_p = [\dots; (X_p^l)^\top; \dots; (X_p^m)^\top]^\top \in \mathbb{R}^{md}$ , following by a FC layer to obtain  $\gamma = [\dots; (\beta^l)^\top; \dots; (\beta^m)^\top]^\top \in \mathbb{R}^{md}$ , where  $m$  is the number of levels. For convenience, we denote the three kinds of methods as V1, V2, V3, respectively, and the results of these methods are showed in Table 7. These three methods achieve comparable

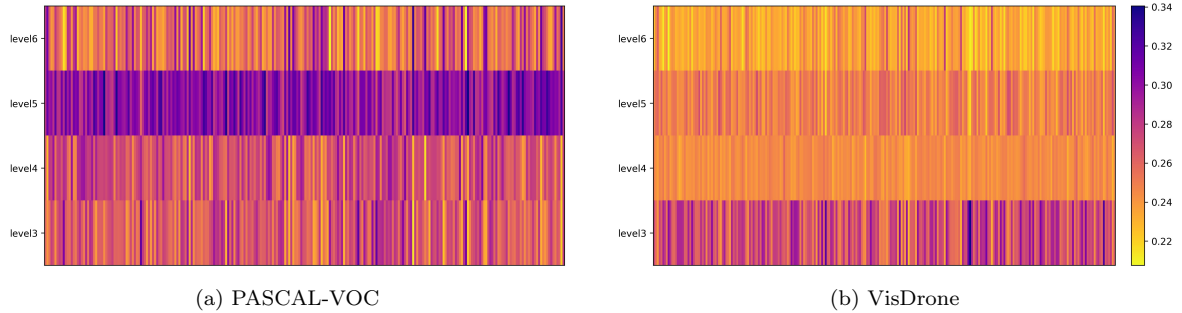


Figure 6: Visualization of the learned weights  $\alpha$  at each level (from level3 to level6). The horizontal axis is the channel dimension, with 256 channels.

Table 6: Comparison of AFSM and ASFF [18]. APs are reported on the VisDrone-DET 2019 *validation* subset.

Method	AP	AP <sup>50</sup>	AP <sup>75</sup>	FPS
Baseline	25.92	46.81	24.75	23.20
+ ASFF	29.15	54.04	27.34	22.34
+ AFSM	<b>29.94</b>	55.40	28.28	22.76

performance, with 29.94%, 29.57%, and 29.79% AP for V1, V2, V3, respectively. However, V1 enjoys the advantages of the fastest inference among the three versions, with an FPS of 21.71. This shows that it is not the ways of obtaining  $\beta^l$  that brings the performance gain, but the mechanism of adaptive feature selection proposed in this paper. The advantages of AFSM are two-fold. On the one hand, it aggregates representations across various feature levels, thus making full use of information on different scales. On the other hand, by applying an importance weight  $\alpha^l$  when aggregating representation at level  $l$ , the model can obtain useful information while relegating the useless parts for the subsequent detection task.

**Visualization of feature selection weights** In order to analyze whether the proposed adaptive feature selection module learns to aggregate useful information from different feature levels, we visualize the learned weights  $\alpha$  at each level as a heatmap. As shown in

Table 7: Different ways of obtaining feature selection weights. The APs are reported on the VisDrone-DET *validation* subset. Baseline is CenterNet with ResNet50 as backbone network, and uses the feature maps at level 3 for the following detection head. Three kinds of methods yield comparable performance, while V1 achieving the fastest inference.

Method	AP	AP <sup>50</sup>	AP <sup>75</sup>	FPS
Baseline	25.92	46.81	24.75	<b>23.20</b>
+ V1	<b>29.94</b>	<b>55.4</b>	<b>28.28</b>	22.76
+ V2	29.57	55.3	27.58	17.77
+ V3	29.79	55.15	28.04	18.02

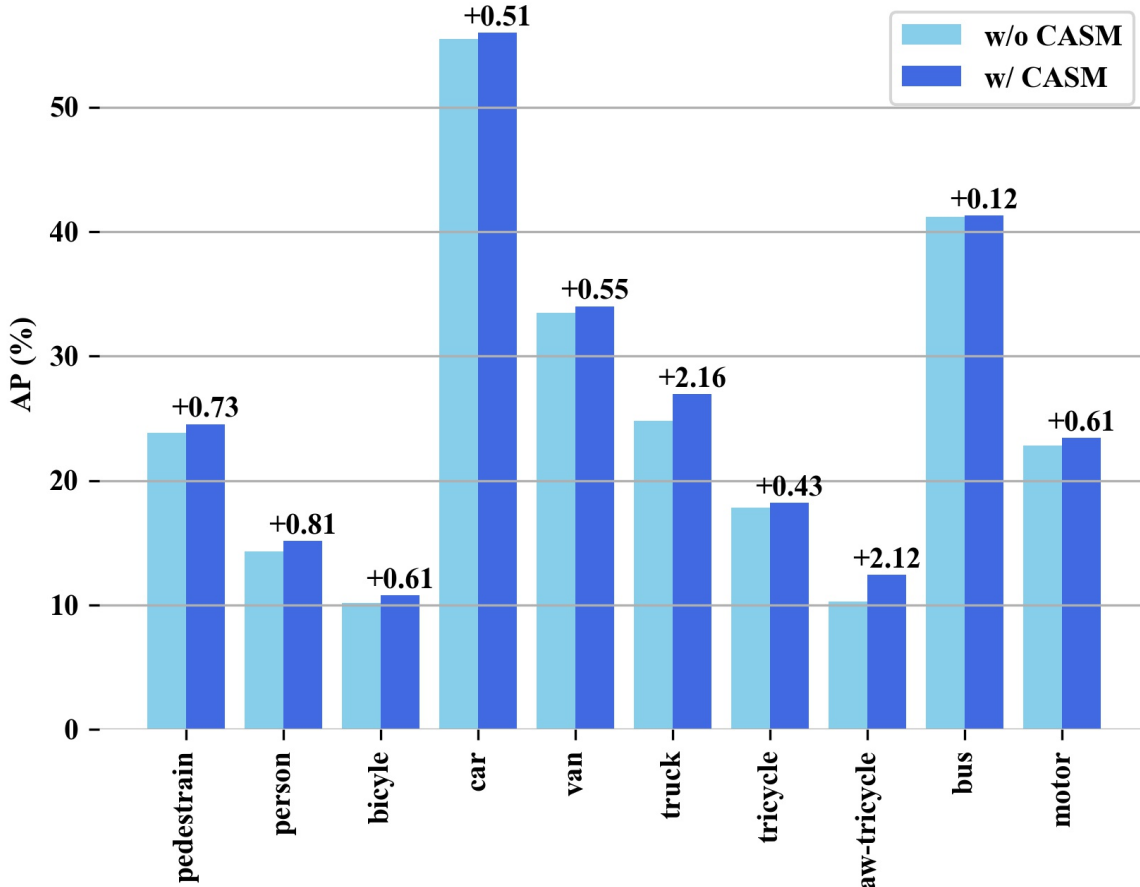


Figure 7: Effect of the class-aware sampling mechanism (CASM). CASM boosts the performance for each of classes, especially for ‘awning tricycle’, with an improvement of 2.12% AP.

Fig. 6, the selection weight  $\alpha^l \in \mathbb{R}^d$  at level  $l$  is exhibited horizontally, where  $d = 256$  in this paper. It can be observed from Fig. 6 that, AFMSM successfully captures the scale distribution of the specific dataset, and learns to adaptively fuse features across multi-scale levels. Specifically, for the VOC dataset, the object scale is relatively uniform and, there is not so much small object. Therefore, the semantic information at high scale level, *e.g.*, level 5, plays a more important role for predicting the large objects, as shown in Fig. 6a. On the other hand, the object scale varies significantly on the VisDrone dataset and, most of them are small objects. It is hence the spatially finer texture information is much beneficial for detecting the vast majority of small objects (see Fig. 6b).

**Effectiveness of the class-aware sampling mechanism** To analyze the effect of the proposed class-aware sampling mechanism, we plot the AP (%) of each class on the VisDrone-DET *validation* subset, with and without CASM. Fig. 7 clearly shows that CASM boosts the performance for each of the classes, especially for the minor classes, *e.g.*, with an improvement of 2.16% and 2.12% AP on ‘truck’ and ‘awning tricycle’, respectively. This demonstrates the effectiveness of CASM, which uplifts the occurrence for minor classes dur-

Table 8: Contribution of AFSM to CornerNet [23] and Faster R-CNN [7]. mAP (%) is reported on VOC 2007 test set. (800, 1333) implies that the shorter size of image is resize to 800, while keeping the longer size within 1333. † means that ResNet50-D [57] is used as backbone network.

Method	Backbone	Resolution	AFSM	mAP	FPS
CornerNet	ResNet50†	511×511		72.13	31.5
CornerNet	ResNet50†	511×511	✓	73.60	30.77
CornerNet	ResNet101	511×511		70.67	29.2
CornerNet	ResNet101	511×511	✓	71.44	27.9
Faster R-CNN	ResNet50†	(800,1333)		81.63	25.23
Faster R-CNN	ResNet50†	(800,1333)	✓	82.06	21.86

ing the training phase, resulting in more supervisory signals and consequently, achieving higher accuracy.

**Evaluation on other detection algorithms** We first instantiate the proposed adaptive feature selection module into the CenterNet detection framework, to evaluate its contribution. However, we emphasize that AFSM is a plug and play module, which can also be applied to other detection algorithms, irrespective of one-stage or two-stage. Therefore, more experiments are carried out on two representative detectors, Faster R-CNN [7] and CornerNet [23]. The former is a state-of-the-art two-stage detector and, the latter is the first to attempt to detect objects with the keypoint estimation method.

The experimental results are showed in Table 8. AFSM consistently increases the performance of two selected detection algorithms, with ResNet50 and ResNet101 as the backbone network. However, it is worth to note that the contribution to CornerNet is more significant, which improves from 72.13% to 73.60%, an increase of 1.47% mAP, when applying AFSM to CornerNet. This is due to the fact that, CornerNet uses a single-scale feature (*i.e.*, level 3) for the subsequent detection head, and AFSM facilitates the detection branch considerably, with the ability to adaptively selecting useful information from various feature scales. On the other hand, Faster R-CNN has already employed FPN for multi-scale object detection, while AFSM can still improve the performance by 0.43% mAP, demonstrating the effectiveness of AFSM.

## 5. Conclusion

This paper aims at tackling two fundamental challenges that limit the performance of object detection algorithms, *i.e.*, the wide range of variation in object scale and the class imbalance problem. To address these challenges, a novel and effective adaptive feature selection module (AFSM) is first proposed, which adaptively learns the selection weight at each scale in the channel dimension, to enhance the important clues at a certain feature level. Secondly, we propose a class-aware sampling mechanism (CASM) to automatically assign the sampling weight to each of the images during training, according to the number of objects in each class. Each of the novel designs can improve the performance of the detector

considerably. Finally, we uplift the baseline to a new state-of-the-art performance, with tiny inference overhead, thanks to the novel proposed methods.

## Acknowledgment

## References

- [1] K. He, X. Zhang, S. Ren, J. Sun, Deep residual learning for image recognition, in: Proceedings of the IEEE conference on computer vision and pattern recognition, 2016, pp. 770–778.
- [2] G. Huang, Z. Liu, L. Van Der Maaten, K. Q. Weinberger, Densely connected convolutional networks, in: Proceedings of the IEEE conference on computer vision and pattern recognition, 2017, pp. 4700–4708.
- [3] K. Simonyan, A. Zisserman, Very deep convolutional networks for large-scale image recognition, arXiv preprint arXiv:1409.1556.
- [4] C. Szegedy, W. Liu, Y. Jia, P. Sermanet, S. Reed, D. Anguelov, D. Erhan, V. Vanhoucke, A. Rabinovich, Going deeper with convolutions, in: Proceedings of the IEEE conference on computer vision and pattern recognition, 2015, pp. 1–9.
- [5] T.-Y. Lin, M. Maire, S. Belongie, J. Hays, P. Perona, D. Ramanan, P. Dollár, C. L. Zitnick, Microsoft coco: Common objects in context, in: European conference on computer vision, Springer, 2014, pp. 740–755.
- [6] M. Everingham, L. Van Gool, C. K. I. Williams, J. Winn, A. Zisserman, The pascal visual object classes (voc) challenge, *International Journal of Computer Vision* 88 (2) (2010) 303–338.
- [7] S. Ren, K. He, R. Girshick, J. Sun, Faster r-cnn: Towards real-time object detection with region proposal networks, in: Advances in neural information processing systems, 2015, pp. 91–99.
- [8] J. Redmon, S. Divvala, R. Girshick, A. Farhadi, You only look once: Unified, real-time object detection, in: Proceedings of the IEEE conference on computer vision and pattern recognition, 2016, pp. 779–788.
- [9] T.-Y. Lin, P. Goyal, R. Girshick, K. He, P. Dollár, Focal loss for dense object detection, in: Proceedings of the IEEE international conference on computer vision, 2017, pp. 2980–2988.
- [10] B. Singh, L. S. Davis, An analysis of scale invariance in object detection snip, in: Proceedings of the IEEE conference on computer vision and pattern recognition, 2018, pp. 3578–3587.
- [11] W. Liu, D. Anguelov, D. Erhan, C. Szegedy, S. Reed, C.-Y. Fu, A. C. Berg, Ssd: Single shot multibox detector, in: European conference on computer vision, Springer, 2016, pp. 21–37.
- [12] T.-Y. Lin, P. Dollár, R. Girshick, K. He, B. Hariharan, S. Belongie, Feature pyramid networks for object detection, in: Proceedings of the IEEE conference on computer vision and pattern recognition, 2017, pp. 2117–2125.
- [13] K. He, G. Gkioxari, P. Dollár, R. Girshick, Mask r-cnn, in: Proceedings of the IEEE international conference on computer vision, 2017, pp. 2961–2969.
- [14] C.-Y. Fu, W. Liu, A. Ranga, A. Tyagi, A. C. Berg, Dssd: Deconvolutional single shot detector, arXiv preprint arXiv:1701.06659.
- [15] S. Woo, S. Hwang, I. S. Kweon, Stairnet: Top-down semantic aggregation for accurate one shot detection, in: 2018 IEEE Winter Conference on Applications of Computer Vision (WACV), IEEE, 2018, pp. 1093–1102.
- [16] S. Zhang, L. Wen, X. Bian, Z. Lei, S. Z. Li, Single-shot refinement neural network for object detection, in: Proceedings of the IEEE conference on computer vision and pattern recognition, 2018, pp. 4203–4212.
- [17] J. Redmon, A. Farhadi, Yolov3: An incremental improvement, arXiv preprint arXiv:1804.02767.
- [18] S. Liu, D. Huang, Y. Wang, Learning spatial fusion for single-shot object detection, arXiv preprint arXiv:1911.09516.
- [19] Q. Zhao, T. Sheng, Y. Wang, Z. Tang, Y. Chen, L. Cai, H. Ling, M2det: A single-shot object detector based on multi-level feature pyramid network, in: Proceedings of the AAAI Conference on Artificial Intelligence, Vol. 33, 2019, pp. 9259–9266.

- [20] J. Hu, L. Shen, G. Sun, Squeeze-and-excitation networks, in: Proceedings of the IEEE conference on computer vision and pattern recognition, 2018, pp. 7132–7141.
- [21] Z. Cai, N. Vasconcelos, Cascade r-cnn: Delving into high quality object detection, in: Proceedings of the IEEE conference on computer vision and pattern recognition, 2018, pp. 6154–6162.
- [22] Y. Wu, Y. Chen, L. Yuan, Z. Liu, L. Wang, H. Li, Y. Fu, Rethinking classification and localization for object detection, in: Proceedings of the IEEE/CVF Conference on Computer Vision and Pattern Recognition, 2020, pp. 10186–10195.
- [23] H. Law, J. Deng, Cornernet: Detecting objects as paired keypoints, in: Proceedings of the European Conference on Computer Vision (ECCV), 2018, pp. 734–750.
- [24] K. Duan, S. Bai, L. Xie, H. Qi, Q. Huang, Q. Tian, Centernet: Keypoint triplets for object detection, in: Proceedings of the IEEE International Conference on Computer Vision, 2019, pp. 6569–6578.
- [25] X. Zhou, D. Wang, P. Krähenbühl, Objects as points, in: arXiv preprint arXiv:1904.07850, 2019.
- [26] X. Zhou, J. Zhuo, P. Krähenbühl, Bottom-up object detection by grouping extreme and center points, 2019 IEEE/CVF Conference on Computer Vision and Pattern Recognition (CVPR) (2019) 850–859.
- [27] J. Long, E. Shelhamer, T. Darrell, Fully convolutional networks for semantic segmentation, in: Proceedings of the IEEE conference on computer vision and pattern recognition, 2015, pp. 3431–3440.
- [28] B. Hariharan, P. Arbeláez, R. Girshick, J. Malik, Hypercolumns for object segmentation and fine-grained localization, in: Proceedings of the IEEE conference on computer vision and pattern recognition, 2015, pp. 447–456.
- [29] S. Liu, L. Qi, H. Qin, J. Shi, J. Jia, Path aggregation network for instance segmentation, in: Proceedings of the IEEE conference on computer vision and pattern recognition, 2018, pp. 8759–8768.
- [30] M. Tan, R. Pang, Q. V. Le, Efficientdet: Scalable and efficient object detection, in: Proceedings of the IEEE/CVF Conference on Computer Vision and Pattern Recognition, 2020, pp. 10781–10790.
- [31] B. Chen, G. Ghiasi, H. Liu, T.-Y. Lin, D. Kalenichenko, H. Adam, Q. V. Le, Mnasfpn: Learning latency-aware pyramid architecture for object detection on mobile devices, in: Proceedings of the IEEE/CVF Conference on Computer Vision and Pattern Recognition, 2020, pp. 13607–13616.
- [32] G. Ghiasi, T.-Y. Lin, Q. V. Le, Nas-fpn: Learning scalable feature pyramid architecture for object detection, in: Proceedings of the IEEE conference on computer vision and pattern recognition, 2019, pp. 7036–7045.
- [33] D. Oñoro-Rubio, M. Niepert, R. J. López-Sastre, Learning short-cut connections for object counting, arXiv preprint arXiv:1805.02919.
- [34] H. Zhang, M. Cisse, Y. N. Dauphin, D. Lopez-Paz, mixup: Beyond empirical risk minimization, arXiv preprint arXiv:1710.09412.
- [35] Y. Cao, J. Xu, S. Lin, F. Wei, H. Hu, Gcnet: Non-local networks meet squeeze-excitation networks and beyond, in: Proceedings of the IEEE International Conference on Computer Vision Workshops, 2019, pp. 0–0.
- [36] H. Rezatofghi, N. Tsoi, J. Gwak, A. Sadeghian, I. Reid, S. Savarese, Generalized intersection over union: A metric and a loss for bounding box regression, in: Proceedings of the IEEE Conference on Computer Vision and Pattern Recognition, 2019, pp. 658–666.
- [37] A. Newell, K. Yang, J. Deng, Stacked hourglass networks for human pose estimation, in: European conference on computer vision, Springer, 2016, pp. 483–499.
- [38] Z. Zhang, T. He, H. Zhang, Z. Zhang, J. Xie, M. Li, Bag of freebies for training object detection neural networks, arXiv preprint arXiv:1902.04103.
- [39] X. Wang, R. Girshick, A. Gupta, K. He, Non-local neural networks, in: Proceedings of the IEEE conference on computer vision and pattern recognition, 2018, pp. 7794–7803.
- [40] P. Zhu, L. Wen, D. Du, X. Bian, Q. Hu, H. Ling, Vision meets drones: Past, present and future, arXiv preprint arXiv:2001.06303.
- [41] Z. Tian, C. Shen, H. Chen, T. He, Fcos: Fully convolutional one-stage object detection, in: Proceedings of the IEEE international conference on computer vision, 2019, pp. 9627–9636.
- [42] J. Zhang, J. Huang, X. Chen, D. Zhang, How to fully exploit the abilities of aerial image detectors, in: Proceedings of the IEEE International Conference on Computer Vision Workshops, 2019, pp. 0–0.

- [43] F. Yang, H. Fan, P. Chu, E. Blasch, H. Ling, Clustered object detection in aerial images, in: Proceedings of the IEEE International Conference on Computer Vision, 2019, pp. 8311–8320.
- [44] Z. Tang, X. Liu, G. Shen, B. Yang, Penet: Object detection using points estimation in aerial images, arXiv preprint arXiv:2001.08247.
- [45] W. Yu, T. Yang, C. Chen, Towards resolving the challenge of long-tail distribution in uav images for object detection, arXiv preprint arXiv:2011.03822.
- [46] X. Zhang, E. Izquierdo, K. Chandramouli, Dense and small object detection in uav vision based on cascade network, in: Proceedings of the IEEE International Conference on Computer Vision Workshops, 2019, pp. 0–0.
- [47] Z. Liu, G. Gao, L. Sun, Z. Fang, Hrdnet: High-resolution detection network for small objects, arXiv preprint arXiv:2006.07607.
- [48] Y. Ma, D. Yu, T. Wu, H. Wang, Paddlepaddle: An open-source deep learning platform from industrial practice, *Frontiers of Data and Computing* 1 (1) (2019) 105–115.
- [49] D. P. Kingma, J. Ba, Adam: A method for stochastic optimization, arXiv preprint arXiv:1412.6980.
- [50] J. Dai, Y. Li, K. He, J. Sun, R-fcn: Object detection via region-based fully convolutional networks, in: *Advances in neural information processing systems*, 2016, pp. 379–387.
- [51] A. Shrivastava, A. Gupta, R. Girshick, Training region-based object detectors with online hard example mining, in: *Proceedings of the IEEE conference on computer vision and pattern recognition*, 2016, pp. 761–769.
- [52] Y. Zhu, C. Zhao, J. Wang, X. Zhao, Y. Wu, H. Lu, Couplenet: Coupling global structure with local parts for object detection, in: *Proceedings of the IEEE international conference on computer vision*, 2017, pp. 4126–4134.
- [53] A. Ghodrati, A. Diba, M. Pedersoli, T. Tuytelaars, L. Van Gool, Deepproposal: Hunting objects by cascading deep convolutional layers, in: *Proceedings of the IEEE international conference on computer vision*, 2015, pp. 2578–2586.
- [54] T. Kong, F. Sun, C. Tan, H. Liu, W. Huang, Deep feature pyramid reconfiguration for object detection, in: *Proceedings of the European Conference on Computer Vision (ECCV)*, 2018, pp. 169–185.
- [55] J. Redmon, A. Farhadi, Yolo9000: better, faster, stronger, in: *Proceedings of the IEEE conference on computer vision and pattern recognition*, 2017, pp. 7263–7271.
- [56] Y. Liu, Y. Wang, S. Wang, T. Liang, Q. Zhao, Z. Tang, H. Ling, Cbnet: A novel composite backbone network architecture for object detection., in: *AAAI*, 2020, pp. 11653–11660.
- [57] T. He, Z. Zhang, H. Zhang, Z. Zhang, J. Xie, M. Li, Bag of tricks for image classification with convolutional neural networks, in: *Proceedings of the IEEE Conference on Computer Vision and Pattern Recognition*, 2019, pp. 558–567.